Mechanical Systems and Signal Processing ▮ (▮▮▮▮) ▮▮▮–▮▮▮

Contents lists available at ScienceDirect

Mechanical Systems and Signal Processing

journal homepage: www.elsevier.com/locate/ymssp

Estimation of multiple sound sources with data and model uncertainties using the EM and evidential EM algorithms

Xun Wang [a,b,*], Benjamin Quost [a], Jean-Daniel Chazot [b], Jérôme Antoni [c]

[a] Sorbonne University, Université de Technologie de Compiègne, CNRS, UMR 7253 Heudiasyc – CS 60319 - 60203 Compiègne cedex, France
[b] Sorbonne University, Université de Technologie de Compiègne, CNRS, UMR 7337 Roberval – CS 60319 - 60203 Compiègne cedex, France
[c] University of Lyon, Laboratory of Vibrations and Acoustics, 69621 Villeurbanne cedex, France

ARTICLE INFO

Article history:
Received 17 February 2015
Received in revised form
2 June 2015
Accepted 18 June 2015

Keywords:
Sound source localization
Statistical inference from imprecise data
Belief functions
Evidential EM algorithm

ABSTRACT

This paper considers the problem of identifying multiple sound sources from acoustical measurements obtained by an array of microphones. The problem is solved via maximum likelihood. In particular, an expectation-maximization (EM) approach is used to estimate the sound source locations and strengths, the pressure measured by a microphone being interpreted as a mixture of latent signals emitted by the sources. This work also considers two kinds of uncertainties pervading the sound propagation and measurement process: uncertain microphone locations and uncertain wavenumber. These uncertainties are transposed to the data in the belief functions framework. Then, the source locations and strengths can be estimated using a variant of the EM algorithm, known as the Evidential EM (E2M) algorithm. Eventually, both simulation and real experiments are shown to illustrate the advantage of using the EM in the case without uncertainty and the E2M in the case of uncertain measurement.

1. Introduction

One of the crucial issues in acoustics engineering is to reduce the noise emitted by complex devices, e.g. electric or combustion engines, with a minimum of added mass. The first step of this task is to know and to understand the acoustic behavior of the device in order to focus on the main sound sources and the most annoying frequency bands. Powerful experimental tools for acoustic imaging are able to give a quick overview of the radiation patterns of complex devices. Beamforming [1–6] and Near-field Acoustical Holography (NAH) [7–10] are popular methods dedicated to the aforementioned issue. These approaches are based on pressure measurements obtained from an array of microphones. Beamforming estimates the Direction Of Arrival (DOA) of the plane waves in the farfield case, or the point source location in the near-field case, by maximizing the Delay-and-Sum beamformer, or equivalently by Least Square Estimation (LSE) [1]. In order to cope with the corresponding ill-posed inverse problem, classical Tikhonov regularization can be used to improve the estimation of the source localization [11]. However, beamforming is still restricted due to its limited resolvable source separation in low frequencies and its difficulty to accurately quantify source levels. Alternatively, NAH can be used to backpropagate the sound pressure over a surface near the sound sources. It ensures a higher spatial resolution by taking into account evanescent

* Corresponding author.
E-mail addresses: xun.wang@hds.utc.fr, xunwang00@gmail.com (X. Wang), benjamin.quost@utc.fr (B. Quost), jean-daniel.chazot@utc.fr (J.-D. Chazot), jerome.antoni@insa-lyon.fr (J. Antoni).

http://dx.doi.org/10.1016/j.ymssp.2015.06.011
0888-3270/

waves and a better quantification by properly solving an inverse problem. Statistically Optimized NAH (SONAH) [8,9] method proceeds similarly but its analytical formalism avoids the errors caused by the use of the discrete spatial Fourier transform in NAH. In a recent paper [12], Antoni presented a unified approach of these different acoustic imaging methods. Based on a Bayesian framework, a super-resolution reconstruction of pressure field is made possible by taking into account prior information about the source distribution. However, all these approaches reconstruct the sound field on a specific surface and thus cannot localize point sources in a 3D space.

This paper proposes a maximum likelihood (ML) approach for the problem of sound source identification in a 3D space. The pressure measured by a microphone is interpreted as a mixture of signals emitted by the various sources. The parameters to estimate are then the locations and strengths of the sources. In the case of a single source, estimating these parameters via ML is straightforward and equivalent to classical beamforming. For multiple sources, however, computing ML estimates of the parameters is difficult, the contributions of the various sources to a measured signal being unknown. Clearly, should these contributions be known, ML estimation would be straightforward as in the single source case. Therefore, Feder and Weinstein [13] proposed to introduce latent variables representing the unknown contributions of the sources to the measured pressures. Then, ML estimates of the model parameters may be obtained via the EM algorithm [14,15]. This algorithm iteratively alternates between two steps: first, the expected source contributions are computed given the current fits of the model parameters; then, these model parameters are updated according to the source contributions newly computed. Similarly, Cirpan and Cikli [16], Kabaoglu et al. [17], Sheng and Hu [18] and Meng et al. [19] investigated the source localization problem using the EM algorithm. However, in all above works, either sound wave attenuation or phase is ignored. In this paper, a more realistic model, where both are considered, is proposed. The sound source estimation problem is then explicitly solved using the EM algorithm.

Contrary to the simulated results presented in the literature, experimental results are always submitted to different kinds of uncertainties [20,21]. In the sound source localization problem, the microphone positions [22–26] and the wavenumber [26–33] in the Green function are never totally certain. Besides, these input parameters can also vary from one measurement to the other, for instance due to motion of the array or to thermal changes. This paper addresses the problem of model estimation from data pervaded by such uncertainties. First and foremost, it should be clear that a distinction is made between randomness and uncertainty. The former stands for irreducible random errors inherent to the environment (such as background and instrumentation noise) and is thus taken into account in the model. The latter corresponds to systematic errors due to an incomplete knowledge of the experimental setting.

Some researchers have investigated how the uncertainties may be taken into account in the sound source localization problem or in other physical models, mainly using propagation of variance [34,35] or error bar [36], probabilistic method [37], Bayesian approaches [38–40,31,41,29,42,43], interval and fuzzy sets analysis [43–46], or belief functions [47,48]. The statistical moment technique coupled with Taylor series expansion [49–51] is frequently used to estimate the output variable uncertainty and some authors [34,35] have used this method to conduct sensitivity and uncertainty analyses in acoustics.

Note that many of the works mentioned above aim at propagating the uncertainty directly through the model. However, sound source estimation is an inverse problem in which imprecise measurements may have a significant impact on the accuracy of the parameter estimates. Some works [31,41,29,38,39] consist in estimating the model in a Bayesian setting by assuming the uncertain parameters as random variables. However, for the case of multiple uncertain parameters and multiple parameters to be estimated, these methods are hardly applicable due to model complexity. Therefore, in order to reduce the model complexity in the uncertainty propagation and parameter estimation, this paper proposes to transfer the uncertainties on some *meta-parameters*[1] of the model, such as microphone locations and wavenumber, to the data level. Then, the resulting uncertain data are used in the estimation process of the model parameters.

The theory of belief functions, also known as Dempster–Shafer theory, is a powerful tool for managing and mining uncertain data. The theory was developed by Dempster and Shafer in Refs. [52–54]. The problem of statistical inference was addressed in Ref. [54] and developed by Denœux [55]. In this latter work, the author proposed a framework in which the data at hand may have been partially or imperfectly observed. Rather than using precise but possibly erroneous data, it is proposed to represent the uncertainty on each measurement using a mathematical tool called contour functions. Then, an extension of the likelihood function and of the EM algorithm, known as the Evidential EM (E2M) algorithm, can be used to maximize the likelihood of such imprecise data. This paper considers uncertainties on some of the meta-parameters such as the temperature of the medium (which has an impact on the wavenumber) and the microphone locations. After the uncertainties on the meta-parameters of the model have been transferred to the data, the E2M algorithm can thus be used to estimate the model parameters.

This article can be seen as a generalization of a previous work [56]. It is organized as follows. Section 2 begins with a description of the model without consideration of uncertainty: the EM algorithm is then used to solve the parameter estimation problem. In particular, the update equations for the model parameters to be estimated (sound source locations and strengths) are provided. Section 3 raises the issue of uncertain measurements, to which the notion of likelihood is extended. Section 4 introduces the E2M algorithm which is used to maximize this generalized likelihood. Section 5 presents experimental results on simulated and real data, with and without taking into account uncertainty. The advantages of the proposed methods are hence demonstrated. Eventually, Section 6 concludes this paper.

[1] By this term, we refer to parameters that are generally considered as known and on which the model implicitly depends.

Please cite this article as: X. Wang, et al., (2015), http://dx.doi.org/10.1016/j.ymssp.2015.06.011

2. Sound source estimation via the EM algorithm

In this section, the sound propagation model is presented first. Then, the model estimation problem is formulated in a statistical framework and solved using the EM algorithm.

2.1. Model

Assume that the acoustic field produced by S sound sources with positions $\mathbf{r}_s$ $(s=1,\ldots,S)$ is measured by an array of M microphones at some known discrete locations $\mathbf{r}'_m$ $(m=1,\ldots,M)$. Fig. 1 displays the problem in the 2D case. The signal measured in the t-th snapshot $(t=1,\ldots,T)$ is the sum of components from different sources, altered by a complex-valued Gaussian distributed [57] noise

$$\mathbf{p}_t = \mathbf{G}(\mathbf{r})\mathbf{A} + \mathbf{n}_t. \tag{1}$$

Here, $\mathbf{p}_t = (p_{1t},\ldots,p_{Mt})^T$ is the vector of measured pressures at a given frequency domain f for a snapshot at time instant t, the vector $\mathbf{A} = (A_1,\ldots,A_s)^T$ contains the strengths of the sound sources, $\mathbf{n}_t = (n_{1t},\ldots,n_{Mt})^T$ is a complex Gaussian distributed noise with 0-mean and covariance matrix $\Sigma = \sigma^2\mathbf{I}_m$, and $\mathbf{G}$ is an M-by-S matrix of Green functions for the Helmholtz operator whose general term g_{ms} describes the sound propagation process

$$g_{ms} = G(\mathbf{r}_s|\mathbf{r}'_m) = \frac{e^{jk|\mathbf{r}_s-\mathbf{r}'_m|}}{4\pi|\mathbf{r}_s-\mathbf{r}'_m|}, \tag{2}$$

where $k=\frac{2\pi f}{c}$ is the wavenumber and c is the sound speed. The sound source localization problem is to estimate the source locations $\mathbf{r}$ and strengths $\mathbf{A}$ given the measurement $\mathbf{p}_t$, $t=1,\ldots,T$.

2.2. Latent source contributions

This section details the solution of the sound source estimation problem presented in Section 2.1. The log-likelihood of Eq. (1) is a function of the source locations $\mathbf{r}$ and strengths $\mathbf{A}$, and of the measured sound pressures $\mathbf{p}=(\mathbf{p}_1,\ldots,\mathbf{p}_T)$; after removing unnecessary constants that do not change its maximum point, it is

$$\log L(\mathbf{r},\mathbf{A}|\mathbf{p}) = -\sum_{t=1}^{T}||\mathbf{p}_t-\mathbf{G}\mathbf{A}||^2. \tag{3}$$

The Maximum Likelihood Estimators (MLE) of $\mathbf{r}$ and $\mathbf{A}$ are obtained by maximizing Eq. (3).

However, this optimization problem can be largely simplified by introducing *latent variables*. A latent variable can be defined as an unknown information that would make the estimation process straightforward, should it be available. Here, the latent variables are the contributions of the various sources to the measured pressures $\mathbf{c}_t=(\mathbf{c}_{1t},\ldots,\mathbf{c}_{St})$, in which

$$\mathbf{c}_{st} = \mathbf{G}_s A_s + \mathbf{n}_{st}. \tag{4}$$

In this equation, $\mathbf{G}_s$ represents the s-th column of the matrix $\mathbf{G}$ and $\mathbf{n}_{st}$ are obtained by arbitrarily decomposing the total noise $\mathbf{n}_t$ into S components, i.e., $\sum_{s=1}^{S}\mathbf{n}_{st}=\mathbf{n}_t$. The relationship between these latent variables (complete data) and the pressures measured by the microphones (therefore referred to as incomplete data) is thus

$$\mathbf{p}_t = \sum_{s=1}^{S}\mathbf{c}_{st}. \tag{5}$$

Finally, by assuming that $\mathbf{n}_{st}$ are mutually independent Gaussian-distributed with mean 0 and covariance matrix $\Sigma_s=\frac{\sigma^2}{S}\mathbf{I}_m$, the log-likelihood of these complete data (after removing unnecessary terms) can be written as

$$\log L(\mathbf{r},\mathbf{A}|\mathbf{c}) = -\sum_{t=1}^{T}\sum_{s=1}^{S}||\mathbf{c}_{st}-\mathbf{G}_s A_s||^2. \tag{6}$$

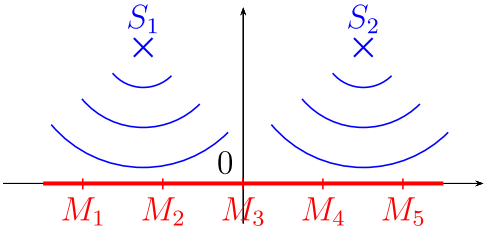

Fig. 1. Sound source estimation problem (2D case). The microphone locations are represented by red points, the sound sources by blue crosses. The origin is assumed here to be the center of the array of microphones. (For interpretation of the references to color in this figure caption, the reader is referred to the web version of this paper.)

Please cite this article as: X. Wang, et al., (2015), http://dx.doi.org/10.1016/j.ymssp.2015.06.011

Intuitively, if the contributions of the sound sources to the measured pressures were available, each source could be treated separately from the others by considering only the corresponding emitted signals in the estimation procedure. Then, the source location and strength could be estimated as in the single source assumption.

2.3. Model estimation via the EM algorithm

Obviously, the complete log-likelihood Eq. (6) cannot be exploited directly, since the latent variables are unknown. The EM algorithm [14] makes it possible to process such missing data by treating them as random variables. Here the basic principle of this algorithm is reviewed and its application in the sound source estimation problem is detailed below.

Let Y be a latent variable with probability density function (pdf) $f_Y(y|\Phi)$, in which Φ is the parameter vector to estimate, and x be an incomplete data obtained from variable X. The idea behind the EM algorithm consists in maximizing the observed log-likelihood by proceeding iteratively with the expected complete log-likelihood given the incomplete data. This latter is obtained by replacing the (missing) latent variables with their expectation, computed using a current fit for the parameter vector Φ. More precisely, the EM algorithm starts from an initial parameter vector Φ^0 and iterates back and forth between two steps:

- in the E-step, the expectation $Q(\Phi|\Phi') = \mathbb{E}(\log f_Y(y|\Phi)|x, \Phi')$ of the complete log-likelihood is computed with respect to the unknown variables given a current fit Φ' for the model parameters;
- the M-step consists in computing a new fit for the parameters by maximizing $Q(\Phi|\Phi')$ with respect to Φ.

It may be shown that, under regularity conditions, the EM algorithm converges towards a local maximum of the observed log-likelihood [14,15]. In order to guarantee the global maximum of the likelihood function, a strategy based on multiple initializations can be employed. The EM algorithm is applied with different initial parameter values that are representatives of the parameter space. Finally, only the result with highest likelihood is retained.

2.3.1. E-step

In the sound source estimation problem, let $\mathbf{r}^l$ and $\mathbf{A}^l$ respectively denote the locations and strengths estimated in the lth iteration of the EM algorithm. Then, the E-step of the $(l+1)$th iteration consists in computing

$$Q(\Phi|\Phi^l) = d - \sum_{t=1}^{T}\sum_{s=1}^{S} ||\mathbb{E}(\mathbf{c}_{st}|\mathbf{p}_t, \mathbf{r}^l, \mathbf{A}^l) - \mathbf{G}_s A_s||^2, \tag{7}$$

where d is a constant independent of $\mathbf{r}$ and $\mathbf{A}$. Before computing the conditional expectation in Eq. (7), the following property [58] is reviewed. Let $\mathbf{X} \sim \mathcal{N}(\mu_\mathbf{X}, \Sigma_{\mathbf{XX}})$ and $\mathbf{Y} \sim \mathcal{N}(\mu_\mathbf{Y}, \Sigma_{\mathbf{YY}})$ be two multivariate Gaussian random vectors. Then, the conditional pdf $f_{\mathbf{Y}|\mathbf{X}}(\cdot|\mathbf{X})$ of $\mathbf{Y}$ given $\mathbf{X}$ is that of a multivariate Gaussian,

$$\mathbf{Y}|\mathbf{X} \sim \mathcal{N}(\mu_\mathbf{Y} + \Sigma_{\mathbf{YX}}\Sigma_{\mathbf{XX}}^{-1}(\mathbf{X} - \mu_\mathbf{X}), \Sigma_{\mathbf{YY}} - \Sigma_{\mathbf{YX}}\Sigma_{\mathbf{XX}}^{-1}\Sigma_{\mathbf{XY}}), \tag{8}$$

where $\Sigma_{\mathbf{XY}} = \mathrm{Cov}(\mathbf{X}, \mathbf{Y})$ and $\Sigma_{\mathbf{YX}} = \mathrm{Cov}(\mathbf{Y}, \mathbf{X})$. Since the observed and complete data are both Gaussian, they are jointly Gaussian, and the conditional expectation of $\mathbf{c}_{st}$ given $\mathbf{p}_t$ is then

$$\hat{\mathbf{c}}_{st}^l = \mathbb{E}\left(\mathbf{c}_{st}|\mathbf{p}_t, \mathbf{r}^l, \mathbf{A}^l\right) = \mathbf{G}_s^l A_s^l + \frac{1}{S}\left(\mathbf{p}_t - \sum_{s=1}^{S} \mathbf{G}_s^l A_s^l\right). \tag{9}$$

This finally gives the following expression for the expectation of the complete log-likelihood:

$$Q(\Phi|\Phi^l) = d - \sum_{t=1}^{T}\sum_{s=1}^{S} ||\hat{\mathbf{c}}_{st}^l - \mathbf{G}_s A_s||^2. \tag{10}$$

2.3.2. M-step

The M-step consists in computing the parameter estimates that maximize Eq. (10):

$$\left(\mathbf{r}_s^{l+1}, A_s^{l+1}\right) = \underset{\mathbf{r}_s, A_s}{\mathrm{argmin}} \sum_{t=1}^{T} ||\hat{\mathbf{c}}_{st}^l - \mathbf{G}_s A_s||^2. \tag{11}$$

These estimates can be determined as follows. For any source locations $\mathbf{r}$,

$$A_s^{l+1} = \underset{A_s}{\mathrm{argmin}} \left|\left|\hat{\mathbf{c}}_s^l - \mathbf{G}_s A_s\right|\right|^2 = \frac{\mathbf{G}_s^H \hat{\mathbf{c}}_s^l}{\mathbf{G}_s^H \mathbf{G}_s}, \tag{12}$$

in which $\hat{\mathbf{c}}_s^l = \frac{1}{T}\sum_{t=1}^{T} \hat{\mathbf{c}}_{st}^l$. Substituting Eq. (12) back into Eq. (11), the source location can be estimated by

$$\mathbf{r}_s^{l+1} = \underset{\mathbf{r}_s}{\operatorname{argmin}} \left\| \hat{\mathbf{c}}_s^l - \frac{\mathbf{G}_s \mathbf{G}_s^H}{\mathbf{G}_s^H \mathbf{G}_s} \hat{\mathbf{c}}_s^l \right\|^2 = \underset{\mathbf{r}_s}{\operatorname{argmax}} (\hat{\mathbf{c}}_s^l)^H \frac{\mathbf{G}_s \mathbf{G}_s^H}{\mathbf{G}_s^H \mathbf{G}_s} \hat{\mathbf{c}}_s^l. \tag{13}$$

Algorithm 1 summarizes the strategy that can be employed to estimate the model via the EM algorithm.

Algorithm 1. Sound source estimation via the EM algorithm.

For $l=0$, pick starting values for the parameters $\mathbf{r}^0, \mathbf{A}^0$. For $l \geq 1$:
repeat
obtain $\hat{\mathbf{c}}_{st}^l$ from Eq. (9), for $s = 1, \ldots, S$;
obtain source location estimates $\mathbf{r}_s^{l+1}$ from Eq. (13), for $s = 1, \ldots, S$;
obtain source strength estimates A_s^{l+1} by substituting $\mathbf{r}_s^{l+1}$ back into Eq. (12), for $s = 1, \ldots, S$.
until the relative increase of the observed data log-likelihood (3) is less than a given threshold.

2.4. Comparison of maximum likelihood and beamforming

In this section, the ML approach is compared with beamforming. The conventional (or Bartlett) beamforming technique is based on the single source assumption. The Delay-and-Sum beamformer, for measured pressures $\mathbf{p}_t$, is defined as

$$B_t = \mathbf{w}^H \mathbf{p}_t = \sum_{m=1}^{M} p_{mt} w_m, \tag{14}$$

its power output is then

$$|B_t|^2 = \mathbf{w}^H \mathbf{p}_t \mathbf{p}_t^H \mathbf{w}. \tag{15}$$

Here, the vector of measured pressures $\mathbf{p}_t$ is defined as in Eq. (1), but in the case of a single source ($S=1$). Then, the weights of the microphones are estimated by solving

$$\widehat{\mathbf{w}}_{BF} = \underset{\mathbf{w}}{\operatorname{argmax}} \mathbb{E}(\mathbf{w}^H \mathbf{p}_t \mathbf{p}_t^H \mathbf{w}) = \underset{\mathbf{w}}{\operatorname{argmax}} \left(A^2 |\mathbf{w}^H \mathbf{G}|^2 + \sigma^2 |\mathbf{w}|^2 \right). \tag{16}$$

In order to obtain a non-trivial solution, $\mathbf{w}$ is constrained to $|\mathbf{w}| = 1$, which gives

$$\widehat{\mathbf{w}}_{BF} = \frac{\mathbf{G}}{\sqrt{\mathbf{G}^H \mathbf{G}}}. \tag{17}$$

Substituting Eq. (17) back into Eq. (15), the source location estimated via beamforming is finally

$$\hat{\mathbf{r}} = \underset{\mathbf{r}}{\operatorname{argmax}} \frac{\mathbf{p}_t^H \mathbf{G} \mathbf{G}^H \mathbf{p}_t}{\mathbf{G}^H \mathbf{G}}. \tag{18}$$

In comparison, in the case of a single source, and under the assumption of Gaussian noise with 0-mean and covariance matrix $\sigma^2 \mathbf{I}_m$, the MLE is

$$\left(\hat{\mathbf{r}}, \widehat{A}\right) = \underset{\mathbf{r},\mathbf{A}}{\operatorname{argmin}} ||\mathbf{p}_t - \mathbf{G}(\mathbf{r})A||^2, \tag{19}$$

which finally leads to the same source location estimates as in Eq. (18).

In the case of multiple sources, the beamforming solves the problem in the same way as the single source case: the assumption is still a single source. An $\mathbf{r}$-$|B_t|^2$ colormap is usually employed to localize the sources. For example, the locations corresponding to the S maxima on the colormap can be retained. But this method is theoretically inappropriate. By contrast, the ML approach is still well defined if the number of sources is predefined, and the update equation of the source locations becomes

$$\hat{\mathbf{r}} = \underset{\mathbf{r}}{\operatorname{argmax}} \mathbf{p}_t^H \mathbf{G} \left(\mathbf{G}^H \mathbf{G} \right)^{-1} \mathbf{G}^H \mathbf{p}_t. \tag{20}$$

However, as mentioned at the beginning of this section, Eq. (20) is difficult to solve, unless the problem is simplified using latent variables and solved by the EM algorithm as in Section 2.2. The update equation of the sound source location estimate (Eq. (13)) indicates that each iteration of the EM algorithm actually performs a beamforming projection for various sources.

3. Model uncertainties

In this section, the problem of model uncertainties is addressed. As mentioned in Section 1, this notion should be distinguished from randomness. The latter refers to random errors due to the environment or the experimental setting (e.g., background and instrumentation noise). Such irreducible errors are thus integrated in the model. In this paper, randomness may be identified to the noise which is quantified by the complex Gaussian-distributed noise component in Eq. (1).

Please cite this article as: X. Wang, et al., (2015), http://dx.doi.org/10.1016/j.ymssp.2015.06.011

Uncertainty, however, accounts for systematic errors due to an imperfect knowledge of the experimental setting. For instance, in this work, the locations of the microphones may be imprecisely known. The medium may also be subject to temperature variation, which in turn changes the wavenumber. Uncertainty is frequently left aside, being identified as one of the causes for randomness. As a matter of fact, taking several snapshots in Section 2 is for reducing the bad effect of the random noise on the source estimation. However, no matter how large the amount of snapshots is, the proposed method in Section 2 cannot cope with uncertainties. Following Refs. [22–33], this paper rather claims that the uncertainties should be quantified and taken into account in the estimation process, so as to make the model estimation more robust.

This section describes how uncertain microphone locations and wavenumber may be taken into account using the theory of belief functions. First, basic material of belief functions is reviewed, in particular the mathematical tools used for quantifying uncertainties in the sound propagation model. Then, the likelihood criterion used classically is extended to the case where the data at hand are uncertain. The problem of estimating the model by maximizing this generalized likelihood will be addressed in Section 4.

3.1. Belief functions

3.1.1. Belief functions on finite domains

Belief functions were originally proposed by Dempster in Ref. [52] in order to represent imprecise and uncertain observations using multi-valued functions, also known as random sets or set-valued mappings. This seminal work was then further extended and developed in Refs. [54,59].

Let X be a variable taking values in a finite domain Ω. Partial knowledge about X may be represented by a *mass function* $m: 2^{\Omega} \to [0,1]$, where 2^{Ω} stands for the power set of Ω, such that $\sum_{A \subseteq \Omega} m(A) = 1$. Any subset A of Ω such that $m(A) > 0$ is called a *focal element* of m. Then, $m(A)$ quantifies the degree of belief that the actual value taken by X is A. Two particular cases are of interest:

- when $m(A) = 1$ for some $A \subseteq \Omega$, the mass function m is said to be categorical (if furthermore $A = \Omega$, then m is vacuous);
- if $|A| = 1$ for all $A \subseteq \Omega$ such that $m(A) > 0$, then m is called a Bayesian belief mass; it is then formally equivalent to a probability distribution.

A mass function m may also be represented by its associated *belief* and *plausibility functions*, defined for all $A \subseteq \Omega$ by

$$Bel(A) = \sum_{B \subseteq A} m(B), \quad Pl(A) = \sum_{B \cap A \neq \phi} (B). \tag{21}$$

The property $Bel(A) \leq Pl(A)$ always holds, for all $A \subseteq \Omega$. The belief function $Bel(A)$ and plausibility function $Pl(A)$ are lower and upper bounds on the possibility that the hypothesis A could be true according to the evidence expressed by the mass function m. Furthermore, if m is Bayesian, then $Bel(A) = Pl(A) = m(A)$ for all $A \subseteq \Omega$. Eventually, the function $pl: \Omega \to [0,1]$ such that $pl(\omega) = Pl(\{\omega\})$ is called the *contour function* associated to m^{Ω}.

3.1.2. Belief functions on the real line

In the case of a continuous domain, e.g., $\Omega = \mathcal{R}$, the notion of mass function is replaced by that of mass density function. A mass density is defined as a function m from the set of closed real intervals to $[0, +\infty)$ such that $m([u,v]) = f(u,v)$ for all $u \leq v$, where f is a two-dimensional probability density function with support in $\{(u,v) \in \mathcal{R}^2 : u \leq v\}$. The intervals $[u,v]$ such that $m([u,v]) > 0$ are called the *focal intervals* of m. The contour function pl corresponding to m is defined by the integral

$$pl(x) = \int_{-\infty}^{x} \int_{x}^{+\infty} f(u,v) dv\, du. \tag{22}$$

One important special case of mass density functions are Bayesian mass functions, for which focal intervals are reduced to points. Then, the two-dimensional pdf has the following form: $f(u,v) = p(u)\delta(u-v)$, where p is a univariate pdf and δ is the Dirac delta distribution. In this case, the contour function $pl(x)$ has the same form as a traditional pdf. If p is further assumed to be a Gaussian pdf, then $pl(x)$ is called a Gaussian contour function.

3.2. Model uncertainty representation using belief functions

It is obvious that ignoring the uncertainty on meta-parameters of the model, such as microphone locations, would introduce a bias in the estimates of the model parameters. Indeed, a pressure p_{mt} used in the estimation process is considered as provided by a microphone with location $\mathbf{r}'_m$. Thus, if the microphone is actually closer to the sound sources than it would have been at this assumed location $\mathbf{r}'_m$, then p_{mt} is overestimated with respect to the pressure that should have been measured at $\mathbf{r}'_m$. Conversely, if the microphone is further away than its nominal location, p_{mt} will be underestimated.

It should be stressed out that the uncertainties on the meta-parameters can be reflected through the observed data (here, the measured pressure vector $\mathbf{p}_t$). Thus, rather than integrating the uncertainties on these meta-parameters directly in the

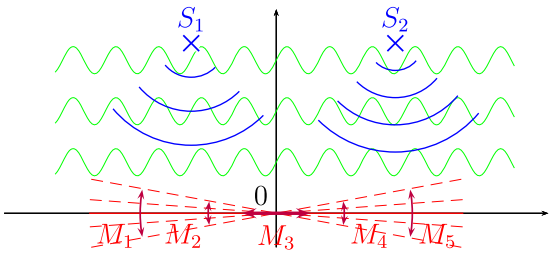

Fig. 2. Sound source estimation problem (2D case) with uncertain meta-parameters (microphone locations and wavenumber).

model, this paper proposes to propagate it to the observed data. This choice is motivated by the efficiency and the versatility of the resulting procedure. Indeed, the propagation step is thus separated from the model estimation process. Furthermore, many kinds of uncertain meta-parameters can then be taken into account, the only requirement is to identify how these uncertainties impact the observed data.

Let the contour function $pl_{\mathbf{p}_t}(\mathbf{p}_t)$ specify the set of plausible values for the pressure measured at time t (for convenience, in the rest of this article $pl_{\mathbf{p}_t}$ is denoted as pl_t). That is, instead of a unique value corresponding to the pressure actually measured, pl_t associates degrees of plausibility to each of the possible pressures. Here, Gaussian contour functions are considered[2]: the imprecise knowledge of the pressure measured is thus quantified by a Gaussian pdf, the expectation of which is assumed to be the measured pressure itself: $\mu_t^* = \mathbf{p}_t$. Its covariance matrix Σ^* directly reflects the level of uncertainty to which the measurement is subject, which can be estimated from the meta-parameter (denoted as $\Theta = (\theta_1, \ldots, \theta_U)$) uncertainties via a first order Taylor approximation [50]

$$\Sigma^* \approx \nabla \mathbf{p}_t(\mu_\Theta) \Sigma_\Theta \nabla \mathbf{p}_t(\mu_\Theta)^H. \tag{23}$$

In this equation, $\nabla \mathbf{p}_t$ is the theoretical gradient related to the measurement $\mathbf{p}_t$ and calculated from the model Eq. (1) with respect to Θ, μ_Θ and Σ_Θ are the expectation and the covariance matrix of Θ. Next, a real-life example of model uncertainties (i.e., the meta-parameters are explicitly given) in the sound source estimation model is considered.

Example 1 (*Imprecise microphone locations and wavenumber*). This example considers a localization problem where the microphone locations are uncertain but their relative positions are precisely known. In this case, the uncertainties on the microphone locations can be decided by the center coordinate and the orientation of the array. Assume also that the wavenumber is subject to uncertainties, for instance due to unmeasurable temperature in the medium. Fig. 2 gives a representation of this problem in a two-dimensional case.

Let the array center be $\mathbf{r}_0 = (x_0, y_0, z_0)$ and the rotation angles around x-, y- and z-axis be θ_1, θ_2 and θ_3. Then, the real coordinates of the microphones can be computed by

$$\mathbf{r}'_m = \mathbf{R}_x(\theta_1)\, \mathbf{R}_y(\theta_2)\, \mathbf{R}_z(\theta_3)(\mathbf{r}^*_m - \mathbf{r}_0), \tag{24}$$

for $m = 1, \ldots, M$, where $\mathbf{r}^*_m$ is the assumed microphone location and the rotation matrices $\mathbf{R}_x$, $\mathbf{R}_y$ and $\mathbf{R}_z$ are defined by

$$\mathbf{R}_x(\theta_1) = \begin{pmatrix} 1 & 0 & 0 \\ 0 & \cos\,\theta_1 & -\sin\,\theta_1 \\ 0 & \sin\,\theta_1 & \cos\,\theta_1 \end{pmatrix}, \tag{25}$$

$$\mathbf{R}_y(\theta_2) = \begin{pmatrix} \cos\,\theta_2 & 0 & -\sin\,\theta_2 \\ 0 & 1 & 0 \\ \sin\,\theta_2 & 0 & \cos\,\theta_2 \end{pmatrix}, \tag{26}$$

$$\mathbf{R}_z(\theta_3) = \begin{pmatrix} \cos\,\theta_3 & -\sin\,\theta_3 & 0 \\ \sin\,\theta_3 & \cos\,\theta_3 & 0 \\ 0 & 0 & 1 \end{pmatrix}. \tag{27}$$

Obviously, these parameters cannot be measured at each time. However, it is reasonable to assume that partial information on the parameter uncertainties is available in the form of variances $\sigma^2_{\theta_1}$, $\sigma^2_{\theta_2}$, $\sigma^2_{\theta_3}$, $\sigma^2_{x_0}$, $\sigma^2_{y_0}$, $\sigma^2_{z_0}$, σ^2_k. Furthermore, these sources of uncertainty are assumed as mutually independent (here it is cognitive independence for variables in the mass assignment space, which means that the belief in one variable does not affect the beliefs in other variables, cf. page 149 in Ref. [54]) and having zero mean (except for the wavenumber which has mean μ_k). Thus, it is proposed to model the meta-parameter uncertainties by a multivariate Gaussian contour function $pl_t(\mathbf{p}_t)$ with expectation $\mu_t^* = \mathbf{p}_t$ and whose covariance

[2] This assumption enables the source estimation in Section 4 to have a closed form. Actually, the distribution of the contour functions can be assumed as other forms, if more information for uncertain data is available.

matrix can be estimated via Eq. (23)

$$\Sigma^* \approx \nabla \mathbf{p}_t(\mu_\Theta)\mathrm{diag}(\sigma_{\theta_1}^2, \sigma_{\theta_2}^2, \sigma_{\theta_3}^2, \sigma_{x_0}^2, \sigma_{y_0}^2, \sigma_{z_0}^2, \sigma_k^2)\nabla \mathbf{p}_t(\mu_\Theta)^H. \tag{28}$$

Here the gradient vector $\nabla \mathbf{p}_t(\mu_\Theta)$ is obtained by Eq. (A.3). The specific computation can be found in Appendix A.

3.3. Likelihood of uncertain data

Let Y denote a continuous random vector taking values in Ω_Y with pdf $p_Y(y|\Phi)$ and y denote a realization of Y, referred to as the complete data. In some cases, y is not precisely observed, but only known that $y \in B$ for some $B \subseteq \Omega_Y$. Then, the likelihood function given such imprecise data is

$$L(\Phi|B) = p_Y(B|\Phi) = \int_{y \in B} p_Y(y|\Phi)\, dy. \tag{29}$$

More generally, the knowledge of y may be not only imprecise, but also uncertain. Such a variable can be described by a contour function pl_Y on Ω_Y. Although partial, the knowledge about the actual realization y of Y is then richer than previously. Then, Denœux [55] proposed to generalize the notion of likelihood function to such uncertain data

$$L(\Phi|pl_Y) = \int_{\Omega_Y} p_Y(y|\Phi) pl_Y(y)\, dy, \tag{30}$$

assuming this integral exists and is nonzero. This generalized likelihood can be considered as a weighted counterpart for Eq. (29): for each possible value y, $p_Y(y|\Phi)$ is weighted according to the degree of plausibility $pl_Y(y)$. Note that when $pl_Y(y) = 1$ for all $y \in B$ and 0 otherwise, Eq. (29) is retrieved.

Here, the variables of interest are the pressures $\mathbf{p}_t$ measured by the microphones. Assume that these pressures are imprecisely known: their partial knowledge can be represented by multivariate contour functions pl_t. In this case, the uncertain data log-likelihood function (corresponding to certain data log-likelihood Eq. (3)) is

$$\log L(\mathbf{r}, \mathbf{A}|pl_t) = \log \int f(\mathbf{p}_t|\mathbf{r}, \mathbf{A}) pl_t(\mathbf{p}_t)\, d\mathbf{p}_t. \tag{31}$$

Assume further that $pl_t(\mathbf{p}_t)$ is Gaussian distributed with mean μ_t^* and covariance matrix Σ^*; the uncertain data log-likelihood then becomes

$$\log L(\mathbf{r}, \mathbf{A}|pl_t) = -(\mu_t^* - \mathbf{GA})^H(\sigma^2\mathbf{I}_m + \Sigma^*)^{-1}(\mu_t^* - \mathbf{GA}). \tag{32}$$

The detailed computation of Eq. (32) may be found in Appendix B.

Example 2. (Log-likelihood of uncertain data) This example considers a simple 2D example to show the advantage of taking into account uncertainties in the data. Fig. 3 displays two sources with actual coordinates $\mathbf{r}_1 = (-1, 2)$ and $\mathbf{r}_2 = (1, 2)$; the coordinates of S_1 and y-coordinate of S_2 are known, so that only the x-coordinate $r_{x,2}$ of S_2 needs to be estimated. Also, five microphones are placed on the y-axis, with assumed x-coordinates $(-2, -1, 0, 1, 2)$. The first four x-coordinates are certain, but the fifth one, written hereafter $m_{x,5}$, is subject to noise and may actually take any value in the interval [1,3] (represented by the pink line segment in Fig. 3). For various user-defined positions of the microphone M_5, pressures are generated by Eq. (1), in which the strengths are $\mathrm{A} = (1, 1)^T$, the frequency f=1000 and the standard deviation of the noise $\sigma = 0.05$. Then, the log-likelihood $\log L(r_{x,2}|\mathbf{p}_t)$ is computed via Eq. (3), *assuming that the microphone position is* (2,0). Alternatively, the generalized log-likelihood $\log L(r_{x,2}|pl_t)$ is computed via Eq. (32), where the Gaussian contour function pl_t has mean μ_t^* taking value as the generated pressure and covariance matrix $\Sigma^* = \mathrm{diag}\left(0, 0, 0, 0, (\sigma_5^*)^2\right)$, with $(\sigma_5^*)^2 \in \{0.003, 0.01, 0.05\}$.

Fig. 4(a) displays the level curves of $\log L(r_{x,2}|\mathbf{p}_t)$ as a function of $r_{x,2}$ and $m_{x,5}$. When the actual microphone x-coordinate is equal to its assumed value ($m_{x,5} = 2$), the log-likelihood of $\mathbf{p}_t$ reaches its maximum for the actual sound source x-coordinate ($r_{x,2} = 1$): in this case, a classical ML estimation makes it possible to correctly locate the sound source. However, when the information of the microphone location is wrong (i.e., $m_{x,5} \neq 2$), this strategy may result in a wrong source location estimate.

Fig. 4(b)–(d) shows the level curves of $\log L(r_{x,2}|pl_t)$ as a function of $r_{x,2}$ and $m_{x,5}$, for $(\sigma_5^*)^2 = 0.003$, $(\sigma_5^*)^2 = 0.01$, and $(\sigma_5^*)^2 = 0.05$, respectively. As the level of uncertainty σ_5^* on the assumed microphone location $m_{x,5}$ increases, it may be seen

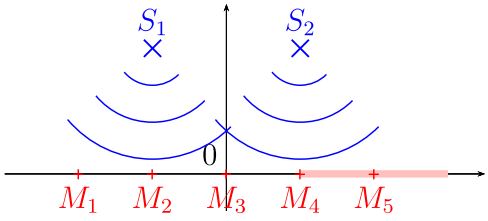

Fig. 3. 2D sound source localization example. The sound sources are represented by blue crosses. The actual microphone locations are represented by red crosses. The real location of 5th microphone is uncertain, taking possible values on pink line segment. (For interpretation of the references to color in this figure caption, the reader is referred to the web version of this paper.)

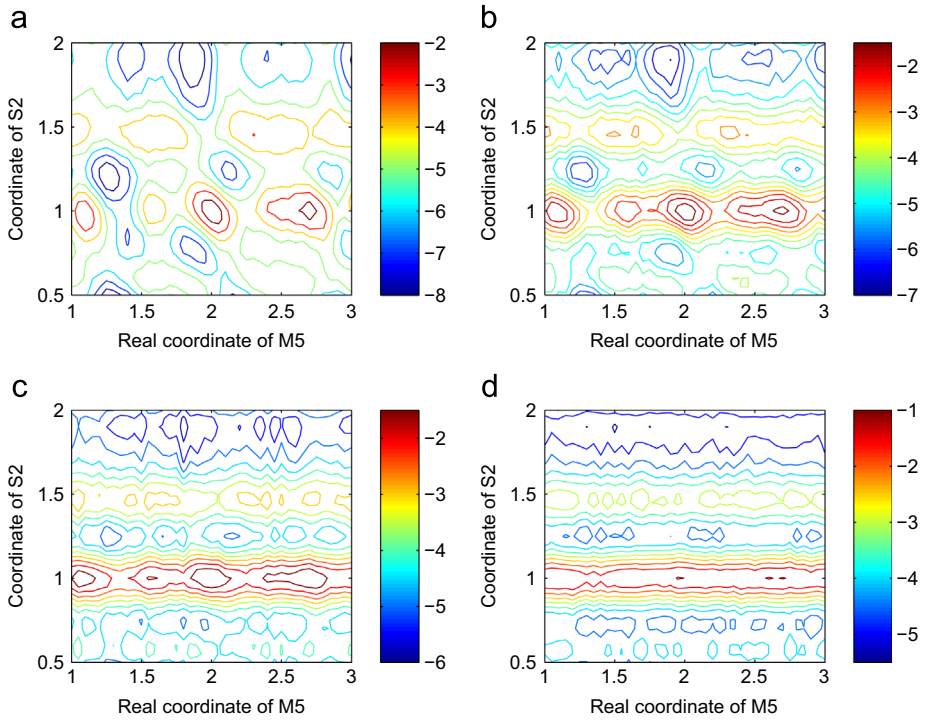

Fig. 4. Log-likelihood of $\mathbf{p}_t$ (a); generalized log-likelihood pl_t (b–d) for different source x-coordinates of S_2 and actual locations of microphone M_5. The values of $(\sigma_5^*)^2$ in pl_t are 0.003, 0.01 and 0.05 in (b), (c) and (d) respectively. In all cases, microphone M_5 is assumed to have a x-coordinate $m_{x,5}=2$.

that the local maxima observed for the classical log-likelihood function disappear. The explanation is that the weight of the information provided by microphone M_5 in the estimation process then decreases. Thus, the estimation process relies more on the information provided by the other microphones, the likelihood function being "smoothed" with respect to the variations of $m_{x,5}$. As a result, maximizing the generalized likelihood makes it possible to correctly estimate the actual sound source location, even if the information provided by M_5 is inaccurate.

4. Sound source estimation in presence of model uncertainty

4.1. Evidential EM algorithm

This section addresses the problem of estimating the model parameters via the ML when the uncertain data at hand are represented using contour functions. Obviously, the EM algorithm cannot be used to maximize the generalized likelihood Eq. (30), since the data are uncertain. An extension of the EM algorithm, known as the Evidential EM (E2M) algorithm, was proposed in Ref. [55] to address this case. Here the principle of this algorithm is briefly reviewed; for an extensive presentation, the readers are invited to refer to Ref. [55].

The E2M algorithm iterates alternatively between two steps. In the E-step of iteration $l+1$, the expectation of the log-likelihood of the complete data given its contour function is computed

$$Q(\Phi|\Phi^l)=\mathbb{E}\left(\log L(\Phi|y)|pl_Y,\Phi^l\right). \tag{33}$$

Note that this expectation is now computed with respect to both the current fit Φ^l of the parameter vector and the contour function pl_Y through which the uncertain sample is known. As explained in Ref. [55], the pdf used in this expectation is defined by

$$p_Y\left(y|pl_Y,\Phi^l\right)=\frac{p_Y(y|\Phi^l)pl_Y(y)}{L(\Phi^l|pl_Y(y))}. \tag{34}$$

Then, Eq. (33) is computed using the definition of the mathematical expectation

$$Q(\Phi|\Phi^l)=\int_{\Omega_Y}\log L(\Phi|y)p_Y(y|pl_Y(y),\Phi^l)\,dy. \tag{35}$$

The M-step of the E2M algorithm is unchanged and requires the maximization of $Q(\Phi|\Phi^l)$ with respect to Φ. As in the EM algorithm, the E2M algorithm alternately repeats the E- and M-steps defined above until the relative increase of the observed-data likelihood becomes smaller than a given threshold.

4.2. Sound source model estimation from uncertain data

In this section, the sound source model presented in Section 2.1 is considered, in the case of uncertain data represented by contour functions pl_t. The generalized likelihood $L(\mathbf{r},\mathbf{A}|pl_t)$ defined in Section 3.3 needs to be maximized. By introducing latent variables (i.e., the contributions $\mathbf{c}_{st}$ of the various sources) such as in Eq. (4), the problem of estimating the model parameters can be solved using the E2M algorithm. We proceed here with the E- and M-steps of this algorithm.

4.2.1. E-step

First, let us notice that

$$Q(\Phi|\Phi^l) = d - \sum_{t=1}^{T}\sum_{s=1}^{S} ||\mathbb{E}(\mathbf{c}_{st}|pl_t,\mathbf{r}^l,\mathbf{A}^l) - \mathbf{G}_s\mathbf{A}_s||^2, \tag{36}$$

where d is a constant independent of $\mathbf{r}$ and $\mathbf{A}$. This expectation depends on the uncertain data only through the expected latent pressures $\hat{\mathbf{c}}_{st} = \mathbb{E}(\mathbf{c}_{st}|pl_t)$. To proceed with the latter, the conditional pdf of the observed pressures given the uncertain data has to be explicitly given

$$f\left(\mathbf{p}_t\middle|pl_t\right) = \frac{pl_t(\mathbf{p}_t)f(\mathbf{p}_t)}{\int pl_t(\mathbf{p}_t)f(\mathbf{p}_t)\,d\mathbf{p}_t}, \tag{37}$$

where $f(\mathbf{p}_t) = \phi(\mathbf{p}_t|\mathbf{GA},\Sigma)$ and $\phi(\cdot|\mu,\Sigma)$ denotes the multivariate Gaussian pdf with expectation μ and covariance matrix Σ. By Eq. (8),

$$f\left(\mathbf{c}_{st}\middle|\mathbf{p}_t\right) = \phi\left(\mathbf{c}_{st}\middle|\mathbf{G}_sA_s + \frac{1}{S}(\mathbf{p}_t - \mathbf{GA}), \left(\frac{1}{S} - \frac{1}{S^2}\right)\Sigma\right). \tag{38}$$

Thus, the conditional pdf of the latent contributions $\mathbf{c}_{st}$ given the uncertain pressures pl_t is

$$f(\mathbf{c}_{st}|pl_t) = \int f(\mathbf{c}_{st}|\mathbf{p}_t)f(\mathbf{p}_t|pl_t)\,d\mathbf{p}_t. \tag{39}$$

Finally, the expectation $\hat{\mathbf{c}}_{st}$ of the latent contributions $\mathbf{c}_{st}$ given the uncertain measured pressures pl_t is

$$\begin{aligned}\hat{\mathbf{c}}_{st} &= \int \mathbf{c}_{st} f\left(\mathbf{c}_{st}|pl_t\right)\,d\mathbf{c}_{st} = \int\int \mathbf{c}_{st} f\left(\mathbf{c}_{st}|\mathbf{p}_t\right)\,d\mathbf{c}_{st} f\left(\mathbf{p}_t|pl_t\right)\,d\mathbf{p}_t \\ &= \mathbf{G}_sA_s - \frac{1}{S}\mathbf{GA} + \frac{1}{S}\frac{\int \mathbf{p}_t pl_t(\mathbf{p}_t)f(\mathbf{p}_t)\,d\mathbf{p}_t}{\int pl_t(\mathbf{p}_t)f(\mathbf{p}_t)\,d\mathbf{p}_t}.\end{aligned} \tag{40}$$

At the $(l+1)$-th iteration, the E-step amounts to computing the expected latent contributions of the sources

$$\hat{\mathbf{c}}_{st}^l = \mathbf{G}_s^lA_s^l - \frac{1}{S}\mathbf{G}^l\mathbf{A}^l + \frac{1}{S}\frac{\int \mathbf{p}_t pl_t(\mathbf{p}_t)f(\mathbf{p}_t|\mathbf{r}^l,\mathbf{A}^l)\,d\mathbf{p}_t}{\int pl_t(\mathbf{p}_t)f(\mathbf{p}_t|\mathbf{r}^l,\mathbf{A}^l)\,d\mathbf{p}_t}. \tag{41}$$

Note that in the general case, computing the last term on the right-hand side of Eq. (40) may be difficult, depending on the form of the contour functions considered. Then, it may require using approximation techniques such as Monte-Carlo estimation. However, if the uncertain measured pressures are represented by Gaussian contour functions $pl_t(\mathbf{p}_t) = \phi(\mathbf{p}_t|\mu_t^*,\Sigma^*)$, a closed form may be obtained.

First, a well-known property of multivariate Gaussians [60] is reviewed here. Assume that $\mathbf{X}$ follows a complex Gaussian distribution with pdf $f_{\mathbf{X}}(\cdot) = \phi(\cdot|\mu_1,\Sigma_1)$ and that it is imprecisely observed through a Gaussian contour function $pl_{\mathbf{X}}(\cdot) = \phi(\cdot|\mu_2,\Sigma_2)$. Then,

$$f_{\mathbf{X}}(\mathbf{x})pl_{\mathbf{X}}(\mathbf{x}) = \phi(\mathbf{x}|\mu_3,\Sigma_3)\phi(\mu_1|\mu_2,\Sigma_1+\Sigma_2) \tag{42}$$

and thus

$$f(\mathbf{x}|pl_{\mathbf{X}}) = \phi(\mathbf{x}|\mu_3,\Sigma_3), \tag{43}$$

where $\mu_3 = (\Sigma_1^{-1}+\Sigma_2^{-1})^{-1}(\Sigma_1^{-1}\mu_1+\Sigma_2^{-1}\mu_2)$ and $\Sigma_3 = (\Sigma_1^{-1}+\Sigma_2^{-1})^{-1}$. Then, from Eqs. (34) and (43), the pdf of the measured pressure vector $\mathbf{p}_t$ given the uncertain measurement pl_t is defined by

$$f(\mathbf{p}_t|pl_t,\mathbf{r}^l,\mathbf{A}^l) = \phi(\mathbf{p}_t|\mu_4,\Sigma_4), \tag{44}$$

Please cite this article as: X. Wang, et al., (2015), http://dx.doi.org/10.1016/j.ymssp.2015.06.011

in which

$$\mu_4 = \left(\frac{\mathbf{I}_m}{\sigma^2} + (\Sigma^*)^{-1}\right)^{-1} \left((\Sigma^*)^{-1}\mu_t^* + \frac{\mathbf{I}_m}{\sigma^2}\mathbf{G}^l\mathbf{A}^l\right), \tag{45}$$

$$\Sigma_4 = \left(\frac{\mathbf{I}_m}{\sigma^2} + (\Sigma^*)^{-1}\right)^{-1}. \tag{46}$$

This makes it possible to get the following expression for the expectations of the latent contributions of the sources

$$\hat{\mathbf{c}}_{st}^l = \mathbf{G}_s^l A_s^l - \frac{1}{S}\mathbf{G}^l\mathbf{A}^l + \frac{1}{S}\mu_4. \tag{47}$$

4.2.2. M-step

The M-step consists in computing new fits for the parameters so as to maximize Eq. (36), or equivalently to solve

$$\mathbf{r}_s^{l+1}, \mathbf{A}_s^{l+1} = \underset{\mathbf{r}_s, A_s}{\operatorname{argmin}} \sum_{t=1}^{T} ||\hat{\mathbf{c}}_{st}^l - \mathbf{G}_s\mathbf{A}_s||^2. \tag{48}$$

Notice that the only difference between the EM and E2M algorithms lies in the E-step (Eqs. (9) and (41)). The general formulation for the M-step (Eqs. (11) and (48)) is the same. The update equations for the M-step of the E2M algorithm are thus

$$\mathbf{r}_s^{l+1} = \underset{\mathbf{r}_s}{\operatorname{argmax}} (\hat{\mathbf{c}}_s^l)^H \frac{\mathbf{G}_s\mathbf{G}_s^H}{\mathbf{G}_s^H\mathbf{G}_s}\hat{\mathbf{c}}_s^l, \tag{49}$$

$$A_s^{l+1} = \frac{(\mathbf{G}_s^{l+1})^H\hat{\mathbf{c}}_s^l}{(\mathbf{G}_s^{l+1})^H\mathbf{G}_s^{l+1}}, \tag{50}$$

where

$$\hat{\mathbf{c}}_s^l = \frac{1}{T}\sum_{t=1}^{T}\hat{\mathbf{c}}_{st}^l. \tag{51}$$

4.3. Algorithm and properties

The strategy for estimating the locations and strengths of the sound sources using the E2M algorithm is summarized by Algorithm 2.

Algorithm 2. Sound source estimation using the E2M algorithm.

For $l=0$, pick starting values for the parameters $\mathbf{r}^0, \mathbf{A}^0$.
For $l \geq 1$:
repeat
  obtain $\hat{\mathbf{c}}_s^l$ from Eqs. (51) and (41) (or (47) for Gaussian contour function case), $s=1,\ldots,S$;
  obtain source location estimates $\mathbf{r}_s^{l+1}, s=1,\ldots,S$ by Eq. (49);
  obtain source strength estimates $A_s^{l+1}, s=1,\ldots,S$ by Eq. (50).
until the relative increase of the log-likelihood ($\log L(\mathbf{r}, \mathbf{A}|pl_{\mathbf{p}})$ given by Eq. (B.3) in Appendix B) is less than a given threshold.

It is easy to conclude that the E2M algorithm is a generalization of the EM algorithm when addressing the problem of sound source estimation. Indeed, when the data are certain, i.e., pl_t is a Dirac distribution located at the measurement point of the pressure, the last term of Eq. (41) becomes $\frac{1}{S}\mathbf{p}_t$ (here for convenience $\mathbf{p}_t$ represents the measurement as well). Then, Eqs. (9) and (41) are equivalent.

In order to highlight the properties of the E2M algorithm and to show how it affects the results for the sound source estimation problem, a particular case of Gaussian contour functions is considered. Assume that the covariance matrix of pl_t is diagonal: $\Sigma^* = \operatorname{diag}((\sigma_1^*)^2, \ldots, (\sigma_m^*)^2)$. Then, the E-step consists in computing $\hat{\mathbf{c}}_{st}^l = (\hat{c}_{1st}, \ldots, \hat{c}_{Mst})$, in which

$$\hat{c}_{mst} = [\mathbf{G}_s^l A_s^l]_m + \frac{1}{S}\frac{\sigma^2(\mu_{mt}^* - [\mathbf{G}^l\mathbf{A}^l]_m)}{\sigma^2 + (\sigma_m^*)^2}, \tag{52}$$

where $[v]_m$ stands for the m-th entry of vector v. Compared with the E-step of the EM algorithm Eq. (9), the E2M algorithm gives an extra weight $\frac{\sigma^2}{\sigma^2+(\sigma_m^*)^2}$ to decrease the belief of the measurement. More particularly, the weight representing the

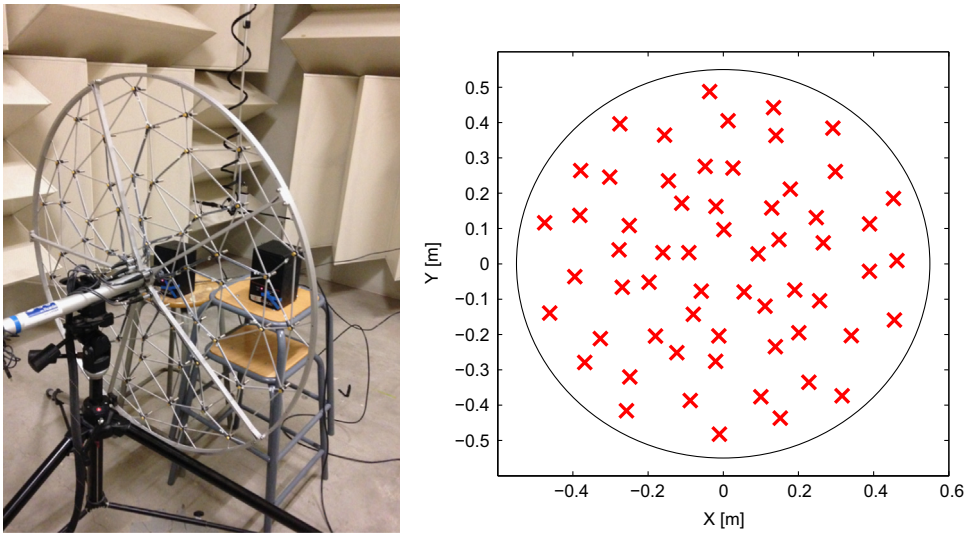

Fig. 5. Experimental setup (left) and microphone distribution (right).

degree of decrease $\frac{\sigma^2}{\sigma^2+(\sigma_m^*)^2} \in (0,1]$ and is decided by the proportion of the variances of the noise and the uncertainty. Moreover, Eq. (52) illustrates that the E2M is a generalization of the EM in terms of level of belief: if the measurement is totally certain, i.e., $(\sigma_m^*)^2 = 0$, the last term of Eq. (52) (E-step) becomes $\frac{1}{S}\left(\mu_{mt}^* - [\mathbf{G}^l\mathbf{A}^l]_m\right)$, which means that the EM and the E2M are identical.

5. Experiments

This section illustrates the proposed methodology on simulated and real data. The experiments are based on the setup described in Fig. 5. An array of 60 microphones is located on the plane $z=0$ (the center of the array coincides with the origin). Two sound sources are placed in front of the microphone array. Note that in the real experiments, these sound sources are surface sources (more precisely, loudspeakers with a vibrating membrane). But in order to numerically assess the accuracy of the estimates using a distance measure, they are assumed as point sources located at the centers of the surfaces.

Section 5.1 presents the experiment realized on real data without uncertainty: the results obtained via the EM-based approach are compared with those given by beamforming and SONAH. In a second time, experiments are realized on data pervaded with uncertain microphone locations and wavenumber. The results are provided in Sections 5.2 and 5.3.

5.1. *Real experiment without uncertainty*

In this experiment, two sound sources (the loudspeakers mentioned previously) are located at $\mathbf{r}_1 = (-0.239, -0.112, 0.314)$ and $\mathbf{r}_2 = (0.172, -0.012, 0.314)$[3], the z-coordinate of which is assumed to be known. Both sources play multi-sine signals with a wide range of frequency (100–6000 Hz). Then, the EM algorithm is run. Figs. 6–8 show the estimation results at different frequencies: in each figure, subplot (a) displays the 100 EM estimates obtained with different initial values (blue points) and the estimates finally retained (red points) that are characterized by the highest likelihood value among the 100 candidates. The initial values are generated as follows. For each source, 100 initial locations $\mathbf{r}_s^0$ are drawn from a two-dimensional uniform distribution with a square 60 cm × 60 cm support centered at the actual position of the source. The initial strength value A_s^0 of each source is generated according to a complex-valued uniform distribution with support in the range of ± 3 dB.

Fig. 6(a) indicates that at low frequencies (lower than 1000 Hz), the EM estimates obtained with the different initial values are almost identical. However, Figs. 7 and 8(a) show that at high frequencies (greater than 1000 Hz), different initial values generally lead to different EM estimates of the sound source locations. Nevertheless, the source location estimates characterized by the highest likelihood value are accurate approximations to the actual ones. Figures (b)–(d) present the sound field reconstructed using the EM estimates, beamforming, and SONAH with Tikhonov regularization, respectively (in the last case, the "optimal" Bayesian regularization parameter is determined as described in Ref. [12]). These results show that beamforming and SONAH can separate the two sources at low frequencies, but give spurious estimates at high frequencies. On the other hand, the EM procedure gives accurate estimates regardless of the frequency considered. Actually, the results of beamforming and SONAH are in line with the well-known limits of both methods. When the frequency is high,

[3] The spatial coordinates are all in meters in this section.

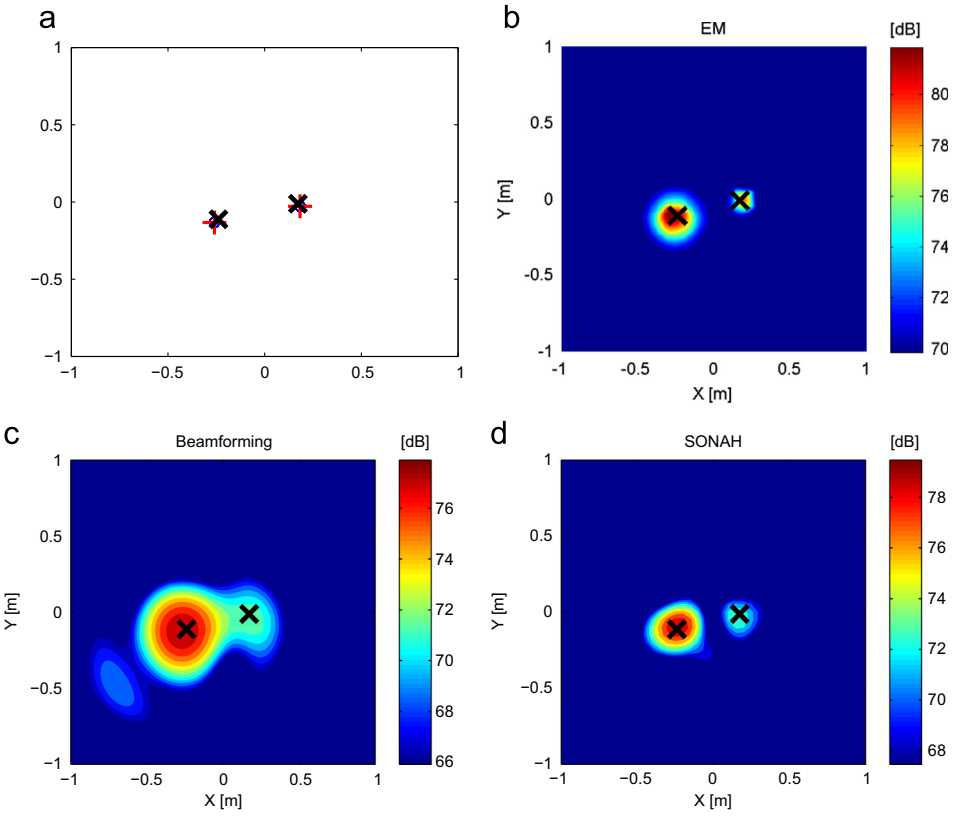

Fig. 6. Estimation results, f=525 Hz. (a) Plot of EM estimates; sound field reconstruction using (b) ML estimates, (c) beamforming, (d) SONAH. Black crosses represent the actual source locations. (For interpretation of the references to color in this figure, the reader is referred to the web version of this paper.)

the acoustical field becomes very complex due to the short wavelength, which means that the non-parametric approaches beamforming and SONAH do not have sufficient spatial measurements to replicate the acoustical field. On the other hand, the EM algorithm is a parametric method: the frequency does not affect the estimation of the sound sources in theory. As a matter of fact, a high frequency brings more local maxima of the likelihood function in a given region, which may also result in an inaccurate estimate (e.g., some blue points in Fig. 8(a)). However, as proposed in Section 2.3, the strategy of multiple initializations can guarantee the convergence of the likelihood function to the global maximum, as well as an accurate estimate of the model parameters. The experimental results justify this approach: 100 initial values can generally guarantee the good results. Moreover, since the EM algorithm converges fast in a few iterations, the computational cost of 100 repeats is still low enough.

5.2. Comparison of EM and E2M on simulated data

Now, uncertainties in the microphone locations and wavenumber are introduced as in Example 1. Two sound sources are considered with strengths $A_1 = A_2 = 0.8$ and locations $\mathbf{r}_1 = (-0.2, 0.1, 0.2)$, $\mathbf{r}_2 = (0.2, -0.1, 0.2)$; the sound frequency is f=5000 Hz for both sources. Then, uncertainties in the microphone locations and the wavenumber are introduced as follows. A wavenumber value is generated according to a Gaussian distribution with mean $\mu_k = \frac{2\pi f}{c}$ (the sound velocity c=340 m/s) and predefined standard deviation σ_k. Similarly, a Gaussian distributed noise is introduced in the array center location $\mathbf{r}_0$ with zero mean and standard deviation $\sigma_{x_0}, \sigma_{y_0}, \sigma_{z_0}$ (for x, y-, z-coordinates respectively) and in each of the rotation angles of the array θ_p ($p = 1, 2, 3$) with mean 0 and predefined standard deviation σ_{θ_p}. Pressures are then generated according to Eqs. (1) and (24), in which $\sigma = 0.05$.

As before, for a given dataset, both the EM and E2M algorithms are run using five different starting values, retaining the solution with highest likelihood. Remark that the covariance matrix Σ^* of the contour functions used in E2M are computed using the parameters $\mathbf{r}$ and $\mathbf{A}$ estimated via the EM algorithm. Since the data are randomly generated, the above procedure (from data generation to model estimation) is repeated 30 times, so that mean square error (MSE) of parameter estimates and 95% confidence intervals of square error may be computed.

First, let $\sigma_{x_0} = \sigma_{y_0} = \sigma_{z_0} = 0.02$, $\sigma_{\theta_p} = 15\frac{\pi}{180}$ for p=1,2,3, σ=0.5. Fig. 9 shows the 30 estimation results for the x- and y-coordinates of the sources via the EM (blue circles) and the E2M (red crosses) algorithms, as well as the 95% confidence

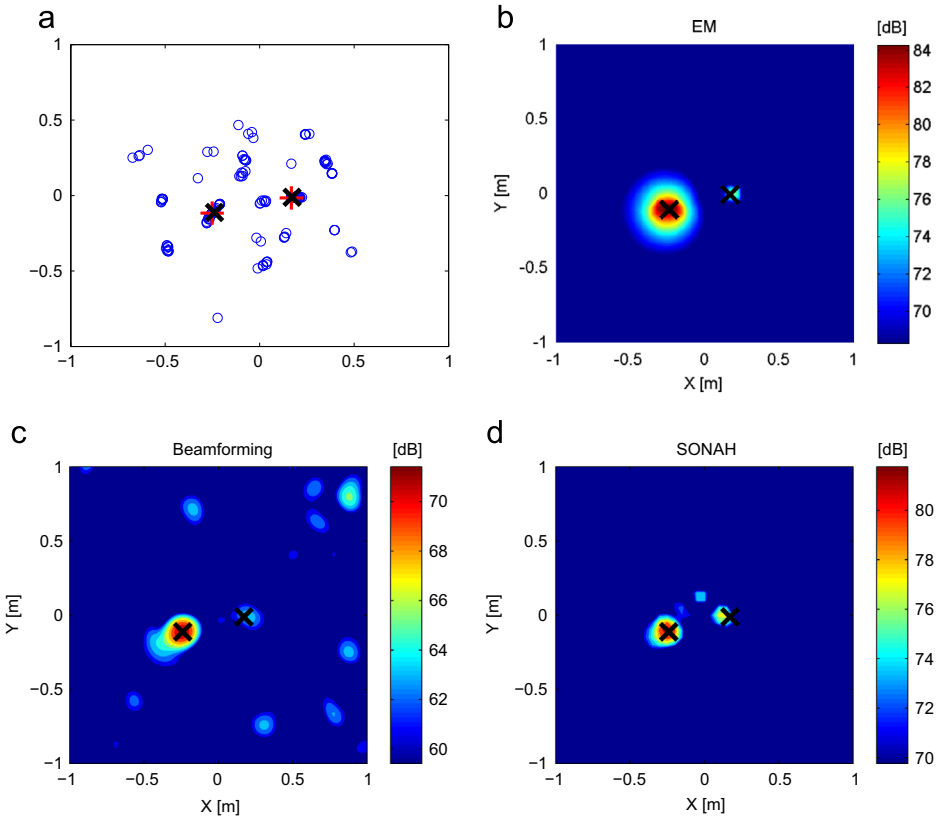

Fig. 7. Estimation results, $f=1325$ Hz. (a) Plot of EM estimates; sound field reconstruction using (b) ML estimates, (c) beamforming, (d) SONAH. Black crosses represent the actual source locations. (For interpretation of the references to color in this figure, the reader is referred to the web version of this paper.)

ellipses of the estimated source location. The estimates obtained via E2M clearly exhibit a smaller spread around the actual sources locations, which illustrates its interest in terms of dealing with uncertain data.

Then, the estimation error of both algorithms are investigated. Let $\sigma_k=0$ (the wavenumber is certain) and let the degree of uncertainty on the microphone locations increase: $\sigma_{x_0}=\sigma_{y_0}=\sigma_{z_0}=0.01l$ and $\sigma_{\theta_p}=5l\frac{\pi}{180}$ ($p=1,2,3$), for $l=0,1,2,3,4$. The MSEs of the estimated sound source locations and 95% confidence intervals of the square errors are displayed in Fig. 10(a). Alternatively, let $\sigma_x=\sigma_y=\sigma_z=\sigma_{\theta_1}=\sigma_{\theta_2}=\sigma_{\theta_3}=0$ (the microphone locations are precise) and let σ_k increase from 0 to 1. Fig. 10(b) shows the corresponding estimation error trend. In both cases, when the level of uncertainty is low, the EM and E2M algorithms exhibit similar performances. As the amount of uncertainty increases, the accuracy of the estimates obtained using both approaches decreases. However, the E2M proves to be much more robust to uncertainty than the EM, its estimation error staying under an acceptable level while the estimation error of EM estimate increases dramatically.

5.3. Comparison of EM and E2M on real data

In this experiment, two sound sources with coordinates $\mathbf{r}_1=(-0.239,-0.112,0.214)$ and $\mathbf{r}_2=(0.172,-0.012,0.214)$ are considered; both radiate at a frequency $f=5025$ Hz. The dataset is composed of 14 different signals: each has a duration of 30 s and is consequently divided and transformed into 30 snapshots in the frequency domain. Uncertainty is introduced in the microphone locations by applying a rotation (around 10° on average) and a translation (around 5 cm on average) to the microphone array. The wavenumber is also considered as uncertain, since the temperature measured during the experiment ranges from 17 °C to 23 °C.

On each of the 14 datasets, ML estimates of the parameters are estimated using both the EM and E2M algorithms, each using 100 initial values obtained as follows. The starting values for each source location are generated using the same protocol as before, according to a three-dimensional uniform distribution on a 10 cm × 10 cm × 5 cm cube. The initial values for the strengths of the sources are generated according to a complex-valued uniform distribution whose support has a range of 6 dB in sound pressure level. The variance σ^2 of measurement noise is estimated by $\frac{1}{M}\sum_{m=1}^{M}\hat{\sigma}_m^2$, in which $\hat{\sigma}_m^2$ is the sample variance of $p_{m1},\ldots,p_{mT}$. Let $\sigma_{\theta_1}=\sigma_{\theta_2}=\sigma_{\theta_3}=\frac{10}{180}\pi$, $\sigma_{x_0}=\sigma_{y_0}=\sigma_{z_0}=0.05$, $\sigma_k=0.3$. For each of the 14 signals, the EM and E2M algorithms are run 100 times with different starting values, and the parameter estimates with highest likelihood are kept.

Please cite this article as: X. Wang, et al., (2015), http://dx.doi.org/10.1016/j.ymssp.2015.06.011

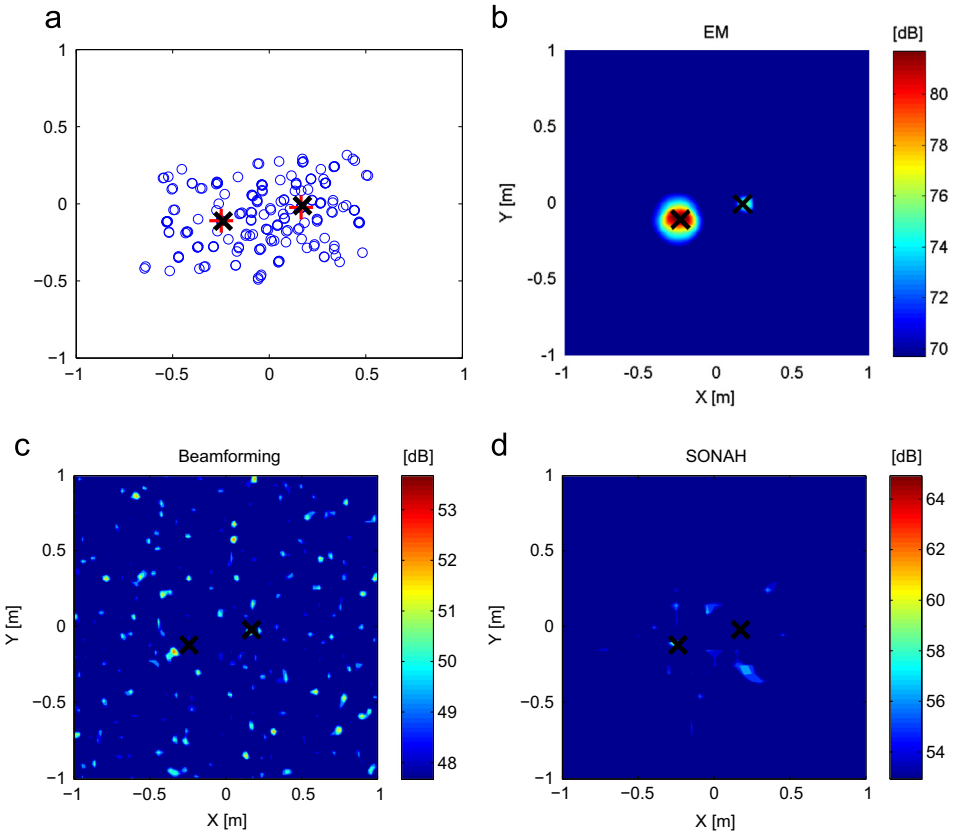

Fig. 8. Estimation results, $f=5025$ Hz. (a) Plot of EM estimates; sound field reconstruction using (b) ML estimates, (c) beamforming, (d) SONAH. Black crosses represent the actual source locations. (For interpretation of the references to color in this figure, the reader is referred to the web version of this paper.)

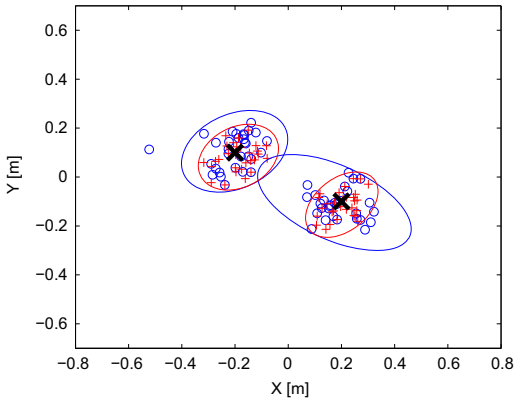

Fig. 9. Source location estimates obtained using the EM (blue) and E2M (red) algorithms and corresponding 95% confidence ellipses. Black crosses stand for the actual locations of the sources. $\sigma_{x_0}=\sigma_{y_0}=\sigma_{z_0}=0.02$, $\sigma_{\theta_1}=\sigma_{\theta_2}=\sigma_{\theta_3}=15\frac{\pi}{180}$, $\sigma_k=0.5$. (For interpretation of the references to color in this figure caption, the reader is referred to the web version of this paper.)

The MSEs of the 14 source location estimates are 0.0435 using EM and 0.0153 using E2M, and the corresponding 95% confidence intervals of the square errors are $[0.0325, 0.0545]$ for EM and $[0.0129, 0.0177]$ for E2M. Furthermore, Fig. 11 displays the x- and y-coordinate estimates along with 95% confidence ellipses of the sources using EM and E2M. Fig. 12 shows the source location estimates and 95% confidence ellipsoids in 3-D space. As before, the E2M estimates exhibit a smaller spread over the actual source locations than the EM estimates. This shows the advantage of taking into account the uncertainty in the model estimation process.

Please cite this article as: X. Wang, et al., (2015), http://dx.doi.org/10.1016/j.ymssp.2015.06.011

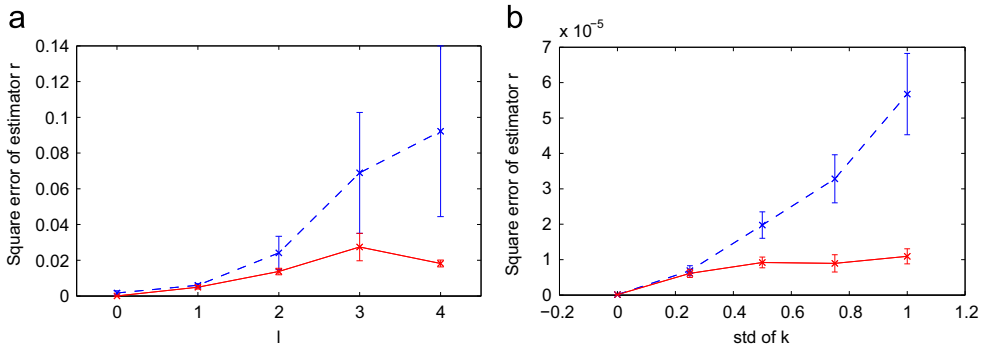

Fig. 10. MSE and 95% confidence intervals for the source location estimates. Case (a): $\sigma_k = 0$, $\sigma_{x_0} = \sigma_{y_0} = \sigma_{z_0} = 0.01$ l, $\sigma_{\theta_1} = \sigma_{\theta_2} = \sigma_{\theta_3} = 5\, l\frac{\pi}{180}$, $l = 0, 1, 2, 3, 4$. Case (b): $\sigma_{x_0} = \sigma_{y_0} = \sigma_{z_0} = \sigma_{\theta_1} = \sigma_{\theta_2} = \sigma_{\theta_3} = 0$, $\sigma_k = 0, 0.25, 0.5, 0.75, 1$.

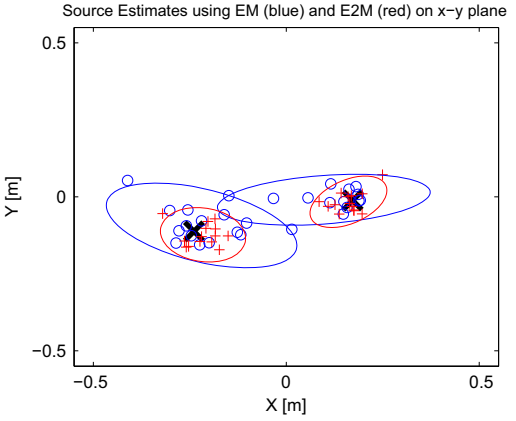

Fig. 11. Source location estimates obtained using EM (blue points) and E2M (red crosses) and corresponding 95% confidence ellipses on the x–y plane. Black crosses represent the actual source locations. (For interpretation of the references to color in this figure caption, the reader is referred to the web version of this paper.)

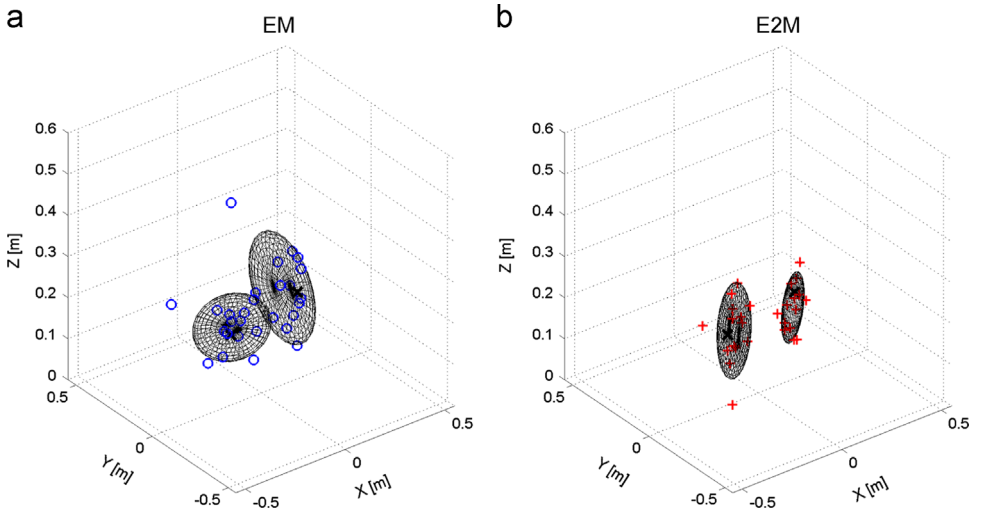

Fig. 12. Source location estimates obtained using EM (left) and E2M (right) and corresponding 95% confidence ellipsoids in 3D space. Black crosses represent the source locations.

6. Conclusions and perspectives

This paper addresses the problem of estimation of multiple sound sources by fitting a propagation model to measured data. The sound pressures are measured by an array of microphones. The sound field is modeled as a free monopole field

with classical Green function. The source estimation problem is then carried out in a statistical framework by maximum likelihood. For this purpose, the contributions of the sources to the measured pressures are considered as latent variables and the EM algorithm is used to solve the maximization problem at a reasonable cost.

A major contribution of this work is the management of uncertain measurements. While randomness is identified as the noise inherent to the measurement process, uncertainty related to ill-known microphone locations and wavenumber is scarcely taken into account in acoustic imaging. Here, uncertainties on the microphone locations and the wavenumber are transposed to the data via first-order approximations. The resulting uncertain pressures are represented using contour functions. Such mathematical objects are defined in the theoretical framework of belief functions as a rich and flexible way to quantify partial knowledge of imperfectly observed variables. Model estimation is carried out by extending the notion of likelihood function to such imprecise data. The resulting generalized likelihood is eventually maximized using an extension of the EM algorithm, known as the Evidential EM algorithm, which was recently proposed for this purpose.

Our approach, which is rather dedicated to engineering applications, is compared with standard methods used in engineering contexts such as beamforming and SONAH. Experimental results obtained on both simulated and r eal data clearly show its interest. The present method is indeed more robust on a larger frequency range than beamforming and SONAH. Besides, the model parameter estimates remain accurate even in presence of uncertain measurements.

Further work may be conducted in several directions. First, the data uncertainties are modeled using Gaussian contour functions in this paper, an assumption which may not always hold. Note that the method proposed in this paper makes it possible to use any kind of contour function: simpler distributions, such as uniform or trapezoidal ones, may give better results when few is known about the data. However, for general contour functions, closed forms for the model parameter estimates may not be obtained, therefore numerical techniques (such as Monte-Carlo integrals) have to be considered. Besides, in the model considered here, the strengths of the sources are assumed to be deterministic. This assumption may be dropped; in this case, the source strengths are considered as random variables, and their distributions are estimated along with the source location parameters via the maximum likelihood. This approach is currently under development.

Acknowledgments

This work was partially funded by the European Union committed in Picardy with the FEDER. It was carried out in the framework of the Labex MS2T, which was funded by the French Government, through the program “Investments for the future” by the National Agency for Research (reference ANR-11-IDEX-0004-02).

Appendix A. Computation of gradient matrix

This appendix derives the gradient matrix $\nabla \mathbf{p}_t(\mu_\Theta)$ in Eq. (28). First let the coordinate of the array center be $\mathbf{r}_0 = (x_0, y_0, z_0)$, the (unknown) actual microphone coordinates be $\mathbf{r}'_m = (x'_m, y'_m, z'_m)$, the assumed microphone coordinates be $\mathbf{r}^*_m = (x^*_m, y^*_m, 0)$, the source coordinates be $\mathbf{r}_s = (x_s, y_s, z_s)$, and $r_{ms} = |\mathbf{r}_s - \mathbf{r}'_m|$. The partial derivatives of the measurement p_{mt} with respect to meta-parameters $\Theta = (\theta_1, \theta_2, \theta_3, x_0, y_0, z_0, k)$ may be computed as

$$\frac{\partial p_{mt}}{\partial \gamma} = \frac{\partial p_{mt}}{\partial x'_m}\frac{\partial x'_m}{\partial \gamma} + \frac{\partial p_{mt}}{\partial y'_m}\frac{\partial y'_m}{\partial \gamma} + \frac{\partial p_{mt}}{\partial z'_m}\frac{\partial z'_m}{\partial \gamma}, \tag{A.1}$$

for all $\gamma \in \{\theta_1, \theta_2, \theta_3, x_0, y_0, z_0\}$, and

$$\frac{\partial p_{mt}}{\partial k} = \sum_{s=1}^{S} \frac{\mathrm{j}A_s}{4\pi} e^{\mathrm{j}kr_{ms}}. \tag{A.2}$$

By computing all the partial derivatives in Eq. (A.1) and taking values at the mean value of the meta parameters $\mu_\Theta = (0, 0, 0, 0, 0, 0, \mu_k)$, Eqs. (A.1) and (A.2) become

$$\frac{\partial p_{mt}}{\partial \theta_1}(\mu_\Theta) = y^*_m \sum_{s=1}^{S} W\frac{z_s}{r^*_{ms}},$$

$$\frac{\partial p_{mt}}{\partial \theta_2}(\mu_\Theta) = x^*_m \sum_{s=1}^{S} W\frac{z_s}{r^*_{ms}},$$

$$\frac{\partial p_{mt}}{\partial \theta_3}(\mu_\Theta) = -y^*_m \sum_{s=1}^{S} W\frac{x_s - x^*_m}{r^*_{ms}} + x^*_m \sum_{s=1}^{S} W\frac{y_s - y^*_m}{r^*_{ms}},$$

$$\frac{\partial p_{mt}}{\partial x_0}(\mu_\Theta) = -\sum_{s=1}^{S} W\frac{x_s - x^*_m}{r^*_{ms}},$$

$$\frac{\partial p_{mt}}{\partial y_0}(\mu_\Theta) = -\sum_{s=1}^{S} W\frac{y_s - y_m^*}{r_{ms}^*},$$

$$\frac{\partial p_{mt}}{\partial z_0}(\mu_\Theta) = -\sum_{s=1}^{S} W\frac{z_s}{r_{ms}^*} \quad \text{and} \quad \frac{\partial p_{mt}}{\partial k}(\mu_\Theta) = \sum_{s=1}^{S} \frac{\mathrm{j}A_s}{4\pi} e^{\mathrm{j}\mu_k r_{ms}^*},$$

in which $W = \frac{A_s}{4\pi}\left[\frac{\mathrm{j}\mu_k}{r_{ms}^*} e^{\mathrm{j}\mu_k r_{ms}^*} - \frac{1}{(r_{ms}^*)^2} e^{-\mathrm{j}\mu_k r_{ms}^*}\right]$ and $r_{ms}^* = \sqrt{(x_s - x_m^*)^2 + (y_s - y_m^*)^2 + z_s^2}$. Denote $\frac{\partial \mathbf{p}_t}{\partial \bullet} = \left(\frac{\partial p_{1t}}{\partial \bullet}, \ldots, \frac{\partial p_{Mt}}{\partial \bullet}\right)^T$, the $M \times 7$ gradient matrix is obtained

$$\nabla \mathbf{p}_t(\mu_\Theta) = \left(\frac{\partial \mathbf{p}_t}{\partial \theta_1}(\mu_\Theta), \frac{\partial \mathbf{p}_t}{\partial \theta_2}(\mu_\Theta), \ldots, \frac{\partial \mathbf{p}_t}{\partial k}(\mu_\Theta)\right). \tag{A.3}$$

Appendix B. Computation of the log-likelihood of the uncertain data

The likelihood function of observed data in the form of contour functions $pl_{\mathbf{p}} = (pl_1, \ldots, pl_T)$ is

$$L(\mathbf{r}, \mathbf{A}|pl_{\mathbf{p}}) = \prod_{t=1}^{T} \int f(\mathbf{p}_t) pl_t(\mathbf{p}_t)\, d\mathbf{p}_t. \tag{B.1}$$

By Eq. (42),

$$\int f(\mathbf{p}_t) pl_t(\mathbf{p}_t)\, d\mathbf{p}_t = \phi(\mu_t^*|\mathbf{GA}, \sigma^2\mathbf{I}_m + \Sigma^*). \tag{B.2}$$

Therefore, the log-likelihood of the uncertain data is obtained

$$\log L(\mathbf{r}, \mathbf{A}|pl_{\mathbf{p}}) = -\sum_{t=1}^{T} (\mu_t^* - \mathbf{GA})^H (\sigma^2\mathbf{I}_m + \Sigma^*)^{-1} (\mu_t^* - \mathbf{GA}). \tag{B.3}$$

References

[1] J.J. Christensen, J. Hald, Technical Review: Beamforming, Bruel & Kjaer, Naerum, 2004.
[2] H. Krim, M. Viberg, Two decades of array signal processing research, IEEE Signal Process. Mag. 13 (4) (1996) 67–94.
[3] B.D. van Veen, K.M. Buckley, Beamforming: a versatile approach to spatial filtering, IEEE Acoust. Speech Signal Process. Mag. 5 (2) (1988) 4–24.
[4] D.H. Seo, J.W. Choi, Y.H. Kim, Impulsive sound source localization using peak and RMS estimation of the time-domain beamformer output, Mech. Syst. Signal Process. 49 (2014) 95–105.
[5] P. Castellini, A. Sassaroli, Acoustic source localization in a reverberant environment by average beamforming, Mech. Syst. Signal Process. 24 (2010) 796–808.
[6] P.A.G. Zavala, W. de Roeck, K. Janssens, J.R.F. Arruda, P. Sas, W. Desmet, Generalized inverse beamforming with optimized regularization strategy, Mech. Syst. Signal Process. 25 (2011) 928–939.
[7] E.G. Williams, Fourier Acoustic: Sound Radiation and Nearfield Acoustical Holography, Academic Press, San Diego, 1999.
[8] R. Steiner, J. Hald, Near-field acoustical holography without the errors and limitations caused by the use of spatial DFT, Int. J. Acoust. Vib. 6 (2001) 83–89.
[9] J. Hald, Basic theory and properties of statistically optimized near-field acoustical holography, J. Acoust. Soc. Am. 125 (4) (2009) 2105–2120.
[10] I.L. Arteaga, R. Scholte, H. Nijmeijer., Improved source reconstruction in Fourier-based near-field acoustic holography applied to small apertures, Mech. Syst. Signal Process. 32 (2012) 359–373.
[11] P.A. Gauthier, C. Camier, Y. Pasco, A. Berry, E. Chambatte, R. Lapointe, M.A. Delalay, Beamforming regularization matrix and inverse problems applied to sound field measurement and extrapolation using microphone array, J. Sound Vib. 330 (2011) 5852–5877.
[12] J. Antoni, A Bayesian approach to sound source reconstruction: Optimal basis, regularization, and focusing, J. Acoust. Soc Am. 131 (4) (2012) 2873–2890.
[13] M. Feder, E. Weinstein, Parameter estimation of superimposed signals using the EM algorithm, IEEE Trans. Acoust. Speech Signal Process. 36 (4) (1988) 477–489.
[14] A.P. Dempster, N.M. Laird, D.B. Rubin, Maximum likelihood from incomplete data via the EM algorithm, J. R. Stat. Soc. Ser. B (Methodol.) 39 (1) (1977) 1–38.
[15] J.C.F. Wu, On the convergence properties of the EM algorithm, Ann. Stat. 11 (1983) 95–103.
[16] H.A. Cirpan, E. Cekli, Deterministic maximum likelihood approach for localization of near-field sources, Int. J. Electron. Commun. 56 (1) (2002) 1–10.
[17] N. Kabaoglu, H.A. Cirpan, E. Cekli, S. Paker, Deterministic maximum likelihood approach for 3-D near-field source localization, Int. J. Electron. Commun. 57 (5) (2003) 345–350.
[18] X. Sheng, Y.H. Hu, Maximum likelihood multiple-source localization using acoustic energy measurements with wireless sensor networks, IEEE Trans. Signal Process. 53 (1) (2005) 44–53.
[19] W. Meng, W. Xiao, L. Xie, An efficient EM algorithm for energy-based multisource localization in wireless sensor networks, IEEE Trans. Instrum. Meas. 60 (3) (2011) 1017–1027.
[20] J.A. Simoen, L.W. Nolte, Wideband optimal a posteriori probability source localization in an uncertain shallow ocean environment, J. Acoust. Soc. Am. 103 (1) (1998) 355–361.
[21] D. Blockley, Analysing uncertainties: towards comparing Bayesian and interval probabilities', Mech. Syst. Signal Process. 37 (2013) 30–42.
[22] T. Ajdler, I. Kozintsev, R. Lienhart, M. Vetterli, Acoustic source localization in distributed sensor network, in: Conference Record of the Thirty-Eighth Asilomar Conference on Signals, Systems and Computers, vol. 2, 2004, pp. 1328–1332.
[23] A. Jakoby, J. Goldberg, H. Messer, Source localization in shallow water in the presence of sensor location uncertainty, IEEE J. Ocean. Eng. 25 (3) (2000) 331–336.
[24] K.C. Ho, X. Lu, L. Kovaisaruch, Source localization using TDOA and FDOA measurements in the presence of receiver location errors: analysis and solution, IEEE Trans. Signal Process. 55 (2) (2007) 684–696.

Please cite this article as: X. Wang, et al., (2015), http://dx.doi.org/10.1016/j.ymssp.2015.06.011

[25] K.C. Ho, L. Yang, On the use of a calibration emitter for source localization in the presence of sensor position uncertainty, IEEE Tran. Signal Process. 56 (12) (2008) 5758–5772.
[26] P. Castellini, M. Martarelli, Acoustic beamforming: analysis of uncertainty and meteorological performances, Mech. Syst. Signal Process. 22 (2008) 672–692.
[27] J. Tabrikian, J.L. Krolik, Robust maximum-likelihood source localization in an uncertain shallow-water waveguide, J. Acoust. Soc. Am. 101 (1) (1997) 241–249.
[28] J. Tabrikian, J.L. Krolik, Barankin bounds for source localization in an uncertain ocean environment, IEEE Trans. Signal Process. 47 (11) (1999) 2917–2927.
[29] E. Shorey, G. de Roeck, G. Lombaert, Dealing with uncertainty in model updating for damage assessment: a review, Mech. Syst. Signal Process. 56–57 (2015) 123–149.
[30] R.M. Hamson, R.M. Heitmeyer, Environmental and system effects on source localization in shallow water by the matched-field processing of a vertical array, J. Acoust. Soc. Am. 86 (5) (1989) 1950–1959.
[31] S.E. Dosso, Environmental uncertainty in ocean acoustic source localization, Inverse Probl. 19 (2003) 419–431.
[32] S. Finette, Embedding uncertainty into ocean acoustic propagation model, J. Acoust. Soc. Am. 117 (3) (2005) 997–1000.
[33] S. Finette, A stochastic representation of environmental uncertainty and its coupling to acoustic wave propagation, J. Acoust. Soc. Am. 120 (5) (2006) 2567–2579.
[34] R. Bussow, B.A.T. Petersson, Path sensitivity and uncertainty propagation in SEA, J. Sound Vib. 300 (2007) 479–489.
[35] Y. Mu, M. Badiey, A.H.D. Cheng, Parameter uncertainty analysis on acoustic response in fluid filled poroelastic media, J. Acoust. Soc. Am. 106 (1) (1999) 151–163.
[36] P.M. Congedo, P. Colonna, C. Corre, J.A.S. Witteveen, G. Iaccarino, Backward uncertainty propagation method in flow problems: application to the prediction of rarefaction shock waves, Comput. Methods Appl. Mech. Eng. 57 (1) (2003) 9–15.
[37] K.R. James, D.R. Dowling, A probability density function method for acoustic field uncertainty analysis, J. Acoust. Soc. Am. 118 (5) (2005) 2802–2810.
[38] E. Zhang, P. Feissel, J. Antoni, A comprehensive Bayesian approach for model updating and quantification of modeling errors, Probab. Eng. Mech. 26 (2011) 550–560.
[39] E. Zhang, J. Antoni, P. Feissel, Bayesian force reconstruction with an uncertain model, J. Sound Vib. 331 (2012) 798–814.
[40] W. Becker, J.E. Oakley, C. Surace, P. Gili, J. Rowson, K. Worden, Bayesian sensitivity analysis of a nonlinear finite element model, Mech. Syst. Signal Process. 32 (2012) 18–31.
[41] A.M. Richardson, L.W. Nolte, A posteriori probability source localization in an uncertain sound speed, deep ocean environment, J. Acoust. Soc. Am. 89 (5) (1991) 2280–2284.
[42] B.J. Yoon, X. Qian, E.R. Dougherty, Quantifying the objective cost of uncertainty in complex dynamical systems, IEEE Trans. Signal Process. 61 (9) (2013) 2256–2266.
[43] W. Zhang, J. Liu, C. Cho, X. Han, A hybrid parameter identification method based on Bayesian approach and interval analysis for uncertain structures, Mech. Syst. Signal Process. 60–61 (2015) 853–865.
[44] S. Adhikari, R. Chowdhury, M.I. Friswell, High dimensional model representation method for fuzzy structural dynamics, J. Sound Vib. 330 (2011) 1516–1529.
[45] R. Chowdhury, S. Adhikari, Fuzzy parametric uncertainty analysis of linear dynamical systems: a surrogate modeling approach, Mech. Syst. Signal Process. 32 (2012) 5–17.
[46] Y.S. Erdogan, P.G. Bakir, Inverse propagation of uncertainties in finite element model updating through use of fuzzy arithmetic, Eng. Appl. Artif. Intell. 26 (2013) 357–367.
[47] C. Gogu, Y. Qiu, S. Segonds, C. Bes, Optimization based algorithms for uncertainty propagation through functions with multidimensional output within evidence theory, J. Mech. Des. 134 (10) (2012) 1–8.
[48] M.E. Riley, Evidence-based quantification of uncertainties induced via simulation-based modeling, Reliab. Eng. Syst. Saf. 133 (2014) 79–86.
[49] P.R. Bevington, D. Keith, Data Reduction and Error Analysis for the Physical Sciences, McGraw-Hill, New York, 2003.
[50] J.C. Clarke, Modeling Uncertainty: A Primer, Tutorial of Oxford University.
[51] D.B. Pengra, Notes on Data Analysis and Experimental Uncertainty, 2009.
[52] A.P. Dempster, Upper and lower probabilities induced by a multivalued mapping, Ann. Math. Stat. 38 (1967) 325–399.
[53] A.P. Dempster, Upper and lower probabilities generated by a random closed interval, J. R. Stat. Soc. Ser. B (Methodol.) 39 (3) (1968) 957–966.
[54] G. Shafer, A Mathematical Theory of Evidence, Princeton University Press, Princeton, N.J., 1976.
[55] T. Denœux, Maximum likelihood estimation from uncertain data in the belief function framework, IEEE Trans. Knowl. Data Eng. 25 (1) (2013) 119–130.
[56] X. Wang, B. Quost, J.D. Chazot, J Antoni, Sound source localization from uncertain information using the evidential EM algorithm, in: 2013 Proceedings of the Seventh International Conference on Scalable Uncertainty Management, SUM 2013, Washington, DC, USA, September, LNAI 8078, Springer-Verlag, 2013, pp. 162–175.
[57] B. Picinbono, Second-order complex random vectors and normal distributions, IEEE Trans. Signal Process. 44 (10) (1996) 2637–2640.
[58] I.B. Rhodes, A tutorial introduction to estimation and filtering, IEEE Trans. Autom. Control AC-16 (6) (1971) 688–706.
[59] P. Smets, Belief functions on real numbers, Int. J. Approx. Reason. 40 (3) (2005) 181–232.
[60] K.B. Petersen, M.S. Petersen, The Matrix Cookbook, 2008.

Please cite this article as: X. Wang, et al., (2015), http://dx.doi.org/10.1016/j.ymssp.2015.06.011